Treating Chemistry in Combustion with Detailed Mechanisms—*In Situ* Adaptive Tabulation in Principal Directions—Premixed Combustion

B. YANG* and S. B. POPE

Sibley School of Mechanical Aerospace Engineering, Cornell University, Ithaca, New York 14853-7501 U.S.A.

A new method to treat chemical reactions in combustion problems with detailed mechanisms is developed. The method is called *in situ* adaptive tabulation in principal directions (ISATPD). The tabulation is done *in situ* during combustion calculations and is made in the first few principal directions of the composition space. The integration of the governing equations of chemical reactions is made using detailed mechanisms. Test calculations of the premixed pairwise mixing stirred reactor (PPMSR) are performed for methane/air combustion with a skeletal mechanism consisting of 16 species and 40 reactions, and for natural gas combustion with the GRI 2.11 mechanism consisting of 49 species and 279 reactions. Results show that this method has excellent accuracy (for all species) and efficiency. A speedup in performing chemistry of 1,665 is obtained for the methane/air combustion system with the skeletal mechanism. The speedup will increase as the calculation continues since less integrations will be performed. © 1998 by The Combustion Institute

1. INTRODUCTION

Chemistry is the most challenging aspect of calculations of reactive flows, laminar or turbulent. Chemistry is essential in calculating reaction flows and at the same time it is the hardest part because usually chemistry introduces a large number of nonlinear differential equations, and the equations are notoriously stiff due to the fact that reactions cover a wide range of time scales.

At present, with existing computational techniques and computer power, a balance has to be made between including detailed chemistry or complex flow patterns. One can either employ detailed chemistry in very simple flows, like calculations of one-dimensional laminar flames [1], or include complex flows with very simple chemistry [2]. Calculations of realistic reactive flows, especially turbulent reactive flows, with detailed chemistry are extremely demanding on computer-time. For example, a calculation of a two-dimensional coflow laminar flame can easily consume 150 h of supercomputer cpu time [3]. For calculations of practical turbulent combustion with detailed chemistry, it may take hundreds of days to perform a PDF calculation [4], and it is not feasible in the foreseeable future to perform a DNS calculation [5]. So simplification methods have been developed in the past to reduce the complexity of chemistry.

Prevailing methods for performing chemistry simplification are the reduced mechanism method [6, 7] and the intrinsic low-dimensional manifold method (ILDM) [8]. The reduced mechanism method is based on assumptions that some species are in steady-state and some reactions are in partial equilibrium. The ILDM method is based on the intrinsic study of underlying time scales of chemical reactions [8]. By equilibrating fast processes with small time scales, one can identify low-dimensional manifolds, thus simplifying the chemistry. Despite the usefulness and success of these methods, there are still some drawbacks and difficulties with them. For the reduced mechanism method, as pointed out in [4, 8], it requires a considerable amount of human time, labor and experience to develop the reduced scheme for each fuel/oxidizer system, or even for the same fuel/oxidizer system under different conditions; the partial equilibrium and steady-state assumptions are not accurate in some regions (e.g., low temperature regions); the errors are not controllable. For the ILDM method, it is not straightforward to parametrize the manifold [4]. In the beginning of the development of the ILDM method, a fixed dimen-

*Corresponding author. Address: 138 Upson Hall, Box XX, Cornell University, Ithaca, New York 14853-7501; E-mail: byang@mae.cornell.edu.

COMBUSTION AND FLAME 112: 85–112 (1998)

Published by Elsevier Science Inc.

0010-2180/98/$19.00
PII S0010-2180(97)00019-9

sion of manifold was used. This introduces errors in the region where a high-dimensional manifold is appropriate. This problem can be overcome by introducing a flow time scale to determine the (variable) dimension of the manifold [4]. In practical computational implementations of results obtained from reduced mechanism or manifold calculations, the method of table-look-up has to be used. The method to generate a table is the same for both reduced mechanism method and the ILDM method. Drawbacks of standard tabulation methods are:

- the whole accessible region of the composition space has to be tabulated since it is not known *a priori* which regions are needed,
- thus the table is very large, especially when the dimension of the table is high,
- when the dimension of the table is high, the work to retrieve information from the table is not trivial.

In this paper, a new method is developed to overcome the above mentioned difficulties with chemistry reduction methods and the tabulation method. We call this new method *in situ* Adaptive Tabulation in Principal Directions (ISATPD). This method has two main parts—the *in situ* adaptive tabulation, and the principal directions. The *in situ* adaptive tabulation method is an efficient tabulation method which can eliminate the difficulties associated with the conventional tabulation method. Doing *in situ* adaptive tabulation in the principal directions of a composition space enables one to use detailed chemistry in calculations of reactive flows. This method is designed for PDF calculations of turbulent combustion. It can also be used in calculations of combustion using other techniques since operator splitting method [9] can always be used to get the species evolution equations only involving chemical reactions.

2. *In situ* ADAPTIVE TABULATION

Let the composition vector be denoted by ϕ, $\phi = \{Y_1, Y_2, \ldots, Y_{n_s}, h\}^T$, where Y_i, $i = 1, 2, \ldots, n_s$, is the mass fraction of species i, n_s is the number of species, and h is the specific enthalpy. Let $n = n_s + 1$. In PDF calculations of turbulent combustion (or calculations using other techniques), by employing fractional step (or operator splitting) methods [9], the governing equations for the composition ϕ involving chemical reactions only can be written as

$$\frac{d\phi}{dt} = \mathbf{S}(\phi), \tag{1}$$

where $\mathbf{S}$ is the source term due to chemical reactions (with enthalpy conservation giving $S_n = 0$).

The question needing to be answered here is this: for a given composition $\phi(t)$ at time t, what is the increment in composition, $\Delta\phi(t)$, due to reactions over a time step δt? In principal, we can directly integrate the ordinary differential equation, Eq. 1 and get the answer. But in practice, since a typical combustion system involves dozens of chemical species and hundreds of chemical reactions, and it is needed to do such integrations many times (e.g., in PDF calculations, it is on the order of 10^9 times), the direct numerical integration of the equations would require a huge amount of supercomputer time (several years) and thus make it impossible in practical use.

To reduce the amount of computer work, the conventional approach is to simplify the chemistry. As mentioned above, two popular methods to do this are the reduced mechanism method and the ILDM method. By using reduced schemes, the complicated chemical reacting system is reduced from $n_s + 1$ dimensional space to a space with low dimensionality, usually around four for reduced mechanism and two for ILDM methods. Results are tabulated. Information in stored in the table. In the table-look-up implementation in calculations of combustion, the increment in composition ϕ is obtained by interpolation of the increments on the surrounding nodes. One major disadvantage of this tabulation method is that one needs to tabulate all possible regions even though most part of the regions may not be accessed by the composition in practical calculations.

The other way to reduce the amount of computer work is the *in situ* adaptive tabulation (ISAT) method. It is based on the idea to tabulate the regions only accessed in calcula-

tions. Thus it reduces the number of integrations and requires less computer work. The ideas of the ISAT method are given in detail in [4] and presented again in the following.

As the PDF calculation is performed, an unstructured table is generated, containing N pairs of compositions and their corresponding increments, $\{\phi^{(j)}, \Delta\phi^{(j)}, j = 1, 2, \ldots, N\}$. The table is stored in a structure that is initially empty ($N = 0$). For each particle on each time step in the PDF calculation, the increment $\Delta\phi$ is sought based on the particle's composition ϕ. The table is searched for an entry $\phi^{(j)}$ sufficiently close to ϕ. If one exists, then $\Delta\phi^{(j)}$ is used to approximate $\Delta\phi$. If a sufficiently close table entry does not exist, then $\Delta\phi$ is computed by the direct integration of Eq. 1, and the result is added to the table.

The ideas of constructing such an unstructured table are illustrated in Fig. 1 for the case of a two-dimensional composition space. For convenience of tabulation, the tabulated region is normalized such that in each direction, the components lie in the region [0, 1]. The composition space is covered by cells. A cell is a rectangle with the cell side to be 2^{-l_i} in direction $i, i = 1, 2$, where l_i is the level in direction i. There are two kinds of cells—the coarse cells (which may be of different sizes) as marked by dashed boxes, and the fine cells (which may be of different sizes) as marked by solid boxes. There is a single composition point that represents each fine cell. For a fine cell, all increments of compositions of points in the cell are accurately represented by the increment of the representative cell point. The accuracy is controlled by the level of a cell. The higher the level, the smaller the cell, and the smaller the approximation error.

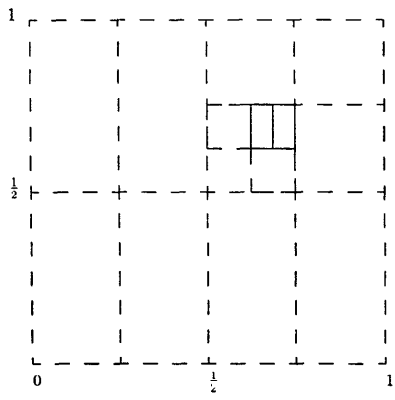

Fig. 1. Cells in the ISAT method.

At the beginning, the table is empty, and the region is covered by a coarse cell which corresponding to level zero. Given a composition $\phi(t)$, the table is searched for a fine cell that contains this composition. If such a fine cell is found (with representative values $\phi^{(j)}$ and $\Delta\phi^{(j)}$, say), then $\Delta\phi^{(j)}$ is returned as an acceptable approximation to the increment $\Delta\phi$. If there is no fine cell containing ϕ, then Eq. 1 is solved to determine $\Delta\phi$ and the pair $\{\phi, \Delta\phi\}$ is added to the table as the representative values of a new fine cell. The level of this new cell is specified. The way to specify the levels is discussed in Section 3.2.

3. THE PRINCIPAL DIRECTIONS OF A COMPOSITION SPACE

The number of fine cells in the table (which we also call the number of records, denoted by n_{rec}) is determined by:

a. the required levels which control the accuracy of the method,

b. the dimensionality of the space in which the tabulation is performed and,

c. the nature of the combustion problem.

There is nothing much we can do about items a and c. With respect to item b, by looking at the singularity of the composition space, we can dramatically decrease the dimension of the space in which tabulation is made. The mathematical tool used here to study the singularity of the composition space is the singular value decomposition (SVD).

3.1. Singular Value Decomposition

The singular value decomposition is a powerful mathematical tool. It enables us to precisely study the matrix rank problem. Here we give the basic idea of SVD. For details of this

method, an excellent mathematical description of this method can be found in [10].

Let $\mathbf{A}$ be a real $m \times k$ matrix, then there exist an $m \times m$ orthogonal matrix $\mathbf{U}$ and a $k \times k$ orthogonal matrix $\mathbf{V}$

$$\mathbf{U} = [\mathbf{u}_1, \mathbf{u}_2, \ldots, \mathbf{u}_m], \tag{2}$$

$$\mathbf{V} = [\mathbf{v}_1, \mathbf{v}_2, \ldots, \mathbf{v}_k], \tag{3}$$

such that

$$\mathbf{U}^T\mathbf{A}\mathbf{V} = \operatorname{diag}(\sigma_1, \sigma_2, \ldots, \sigma_w), \quad w = \min\{m, k\}, \tag{4}$$

where $\sigma_1 \geq \sigma_2 \geq \cdots \geq \sigma_w \geq 0$, $\mathbf{U}^T$ is the transpose of $\mathbf{U}$. The σ_i are the singular values of $\mathbf{A}$. Vectors $\mathbf{u}_i$ and $\mathbf{v}_i$ are the ith left singular vector and the ith right singular vector respectively [10].

Singular values σ_i tell one the precise information of the rank of the matrix $\mathbf{A}$. If l of σ_i are precisely zero, then the rank of the matrix $\mathbf{A}$ is $w - l$. If a singular value σ_j is not exactly zero, but the small number, then the rank of the matrix $\mathbf{A}$ is degenerated almost by one. The value of σ_j tells us to what extend the degeneration is.

3.2. The Principal Directions of a Composition Space

Let ϕ^0 be one composition vector in a composition space ϕ, then we can form the following matrix $\mathbf{C}$:

$$\mathbf{C} = \langle (\phi - \phi^0)(\phi - \phi^0)^T \rangle, \tag{5}$$

where $\langle\ \rangle$ means ensemble average over all accessible composition points. $\mathbf{C}$ is an $n \times n$ symmetric positive semidefinite matrix. Applying the singular value decomposition to the matrix $\mathbf{C}$, then one can write

$$\mathbf{U}^T\mathbf{C}\mathbf{V} = \operatorname{diag}(\sigma_1, \sigma_2, \ldots, \sigma_n), \tag{6}$$

where σ_i are singular values of the matrix $\mathbf{C}$, $\sigma_1 \geq \sigma_2 \geq \cdots \geq \sigma_n \geq 0$. Because of the symmetry of the matrix $\mathbf{C}$, the $n \times n$ orthogonal matrices $\mathbf{U}$ and $\mathbf{V}$ are the same, and the singular values are the eigenvalues, the singular vectors are the eigenvectors. We denote the matrices $\mathbf{U}$ and $\mathbf{V}$ by:

$$\mathbf{U} = [\mathbf{u}_1, \mathbf{u}_2, \ldots, \mathbf{u}_n]. \tag{7}$$

The vectors $\mathbf{u}_1, \mathbf{u}_2, \ldots, \mathbf{u}_n$ are the eigenvectors, or principal axes, of $\mathbf{C}$. We call the directions determined by vectors $\mathbf{u}_1, \mathbf{u}_2, \ldots, \mathbf{u}_n$ the principal directions of the composition space.

Using $\mathbf{u}_1, \mathbf{u}_2, \ldots, \mathbf{u}_n$ as the basis for the composition space, then any composition vector $\phi - \phi^0$ can be written as

$$\phi - \phi^0 = \mathbf{U}\hat{\phi}, \tag{8}$$

we call $\hat{\phi}$ the principal vector of ϕ.

In terms of $\hat{\phi}$, the composition vector ϕ can be written as

$$\phi = \phi^0 + \mathbf{U}\hat{\phi} = \phi^0 + \sum_{j=1}^{n} \hat{\phi}_j \mathbf{u}_j, \tag{9}$$

where $\hat{\phi}_j$, $j = 1, \ldots, n$, are the principal components. For the kth component, $k = 1, \ldots, n$, it can be written as

$$\phi_k = \phi_k^0 + \sum_{j=1}^{n} \hat{\phi}_j u_{j,k}, \tag{10}$$

where ϕ_k^0 is the kth component of ϕ^0, and $u_{j,k}$ is the kth component of the vector $\mathbf{u}_j$. From Eq. 10 one can easily see that ϕ_k is a summation of the kth component of ϕ^0 and the principal components $\hat{\phi}_j$, $j = 1, \ldots, n$, weighted by the kth components of the corresponding principal vectors.

In our test calculations, the tabulation process is like the following (for details, see Section 4.3): for a given composition vector ϕ, find the corresponding principal vector $\hat{\phi}$ according to Eq. 8; then normalize the principal vector such that in each principal direction, the normalized component lies in the region $[0, 1]$; finally, do tabulation in the normalized region. Three different methods of specifying the levels are tested. They are shown in Table 1. For Method I, the levels in principal directions 1, 2, and 3 are 7, 6, 4, respectively, all other principal directions are ignored in the tabulation. A fine cell in Method I is a cuboid with the sides in direction 1, 2, 3 being 2^{-7}, 2^{-6}, and 2^{-4}, respectively.

4. IMPLEMENTATION OF ISATPD METHOD FOR THE PREMIXED PAIRWISE MIXING STIRRED REACTOR

4.1. The Premixed Pairwise Mixing Stirred Reactor

In [4], a premixed pairwise mixing stirred reactor (PPMSR, or PMSR as in [4]) is designed to provide a better test case for chemistry implementation than the partially stirred reactor (PaSR). For a PaSR, the IEM model is used. The mixing occurs between particles and the mean. As a result, the composition of a particle is a unique function of its age. So all particle compositions lie on a simple one-dimensional manifold. For a PPMSR, the mixing takes place between randomly chosen particles. Thus compositions of particles can access a much larger region than that in a PaSR, and so PPMSR provides a more stringent test case.

The description of the PPMSR is given in [4] and repeated here again for the convenience of readers. With Δt being a time step, "reactor events" take place at the discrete times Δt, $2\Delta t, \ldots$. These events consist of outflow, inflow, and pairing. At each event, m_{out} particle pairs (selected at random) flow out of the reactor (i.e., they are discarded). m_{out} is chosen to be the closest integer to $L\Delta t/\tau_{\text{res}}$, where $L = M/2$, M is the number of particles in the reactor, τ_{res} is the residence time. A "candidate pile" is created consisting of $2m_{\text{in}}$ particles with the specified inlet composition (where $m_{\text{in}} = m_{\text{out}}$), and $m_{\text{pair}} = L\,\Delta t/\tau_{\text{pair}}$ pairs randomly selected from the reactor. τ_{pair} is the pairing time scale. Then the particles in the candidate pile are paired randomly, and are then added to the reactor. After this event, the reactor again consists of L pairs of particles.

Between reactor events, the particle compositions evolve continuously. With i and j being the indices of a pair of particles, their compositions evolve according to the equations

$$d\phi^{(i)}/dt = \mathbf{S}(\phi^{(i)}) + (\phi^{(j)} - \phi^{(i)})/\tau_{\text{mix}}, \quad (11)$$

$$d\phi^{(j)}/dt = \mathbf{S}(\phi^{(j)}) + (\phi^{(i)} - \phi^{(j)})/\tau_{\text{mix}}, \quad (12)$$

where $\mathbf{S}$ is the chemical reaction term, and τ_{mix} is the mixing time scale.

In all the calculations in this paper. the parameters are chosen as the following: $M = 100$, $\tau_{\text{res}} = 10^{-2}$ (s), $\tau_{\text{pair}} = 10^{-3}$ (s), $\Delta t = 6.0 \times 10^{-4}$ (s), the temperature of the inflow particles is 300 K. Other parameters are given different values in different test cases.

4.2. Operator Splitting for the Governing Equations

In order to use the table-look-up technique for implementation of chemistry, it is necessary to split Eqs. 11 and 12 such that the increment of composition ϕ depends only on ϕ itself. The mathematical background of operator splitting methods (or fractional step methods) is summarized in [9]. Operator splitting introduces an error called the splitting error, which depends on the value of the time step and on the mixing time in the model shown by Eqs. 11 and 12. The operator splitting error can be decreased by decreasing the time step. So we further divide the time step Δt into several small subtime steps, δt, $\delta t = \Delta t/n_{\text{sub}}$, where n_{sub} is the number of subtime steps.

There are numerous ways to split a system. As suggested in [4], a good splitting approach to split Eqs. 11 and 12 is the zero-order splitting method. For this method, Eqs. 11 and 12 are split into a pure mixing system:

$$d\phi^{(i)}/dt = (\phi^{(j)} - \phi^{(i)})/\tau_{\text{mix}}, \quad (13)$$

$$d\phi^{(j)}/dt = -(\phi^{(j)} - \phi^{(i)})/\tau_{\text{mix}}, \quad (14)$$

and a pure chemical reaction system:

$$d\phi^{(i)}/dt = \mathbf{S}(\phi^{(i)}), \quad (15)$$

$$d\phi^{(j)}/dt = \mathbf{S}(\phi^{(j)}), \quad (16)$$

In the first fractional step, the pure mixing system is integrated (analytic solutions can be obtained) over a time step δt, to get $\phi^{(i)}_{\text{mix}}$ and $\phi^{(j)}_{\text{mix}}$; then, in the second fractional step, the pure reaction system is integrated (from initial conditions $\phi^{(i)}_{\text{mix}}$ and $\phi^{(j)}_{\text{mix}}$) over a time step δt to get the final solutions, $\phi^{(i)}(t + \delta t)$ and $\phi^{(j)}(t + \delta t)$. The second fractional step is the dominant time-consuming part. One can either perform this step by the direct numerical integration of Eqs. 15 and 16, or by table-look-up methods.

4.3. ISATPD for PPMSR Calculations with Detailed Chemistry

In this paper, the second fractional step is carried out by direct integration of the corresponding governing equations and by the ISATPD method. From the results we can compare the accuracy of the ISATPD method.

To use the ISATPD method, we need to know the matrix **C**. If we known all the accessible points in the composition space, then according to Eq. 5, it is easy to get **C**. In practical calculations, this is not possible. Two alternative methods are taken to calculate the matrix **C**. In the first method, direct numerical integrations using zero-order splitting strategy are employed to calculate the PPMSR for a number of time steps. Then the data from this calculation is used to calculate the matrix **C**. The second method is to perform an ignition calculation for the fuel/oxidizer mixture system. Compositions from the initial condition to the equilibrium are used as composition samples to calculate the matrix **C**. Tests show that these two methods have the same accuracy and efficiency.

Once the matrix **C** is obtained, the singular value decomposition is performed for **C** to get the orthogonal matrix **U**. Then from composition vectors ϕ obtained either from direct numerical integration using zero-order splitting strategy or ignition calculations, the corresponding principal vectors, denoted by $\hat{\phi}$, are calculated using $\mathbf{U}^T$. Maximum and minimum values in each direction of $\hat{\phi}$ are found. They are denoted by $\hat{\phi}_{\max}$ and $\hat{\phi}_{\min}$, respectively. The range in each direction is denoted by $\hat{\phi}_r$, and defined by

$$\hat{\phi}_r = \hat{\phi}_{\max} - \hat{\phi}_{\min}. \tag{17}$$

Two chemical kinetic mechanisms are used in this paper. One of them is for the methane/air combustion system, which consists of 16 species and 40 reactions. We call this mechanism the skeletal mechanism. The other mechanism is the GRI 2.11 mechanism for natural gas combustion, which has 49 species and 279 reactions. This mechanism is optimized to best represent the chemical kinetics of natural gas flames, ignition, and NO_x formation and reburning in natural gas combustion. To save the space, these two mechanisms are now shown in this paper. The skeletal mechanism is included in [4]. The GRI 2.11 mechanism can be obtained from the Gas Research Institute.

Typical singular values, σ_i, and the range $\hat{\phi}_r$ are plotted in Fig. 2 for the methane/air combustion system with the skeletal mechanism and in Fig. 3 for the natural gas combustion system with the GRI 2.11 mechanism. For the methane/air combustion system with the skeletal mechanism, there are five conserved quantities (four element conservations, one enthalpy conservation), so there are five zero singular values. The maximum singular value is about unity. Then it decreases rapidly. Looking at the value of the range in each direction, one can find that the last five components are numerically zeros. Figure 2 show that the value of the range decreases rapidly with the increasing in the principal direction. The same statements for the natural gas combustion system with the GRI 2.11 mechanism are also true except that there are six conserved quantities (five element conservations, one enthalpy conservation) instead of five as for the methane/air system with the skeletal mechanism. The extremely important and useful property and consequence of this are:

- mapping the composition vector ϕ into the principal directions by the transpose of the orthogonal matrix **U**, the trajectory of the composition in the principal directions is essentially confined to the first several directions, no matter the original dimension of the composition space is 16 or 49, as for the mechanism tested. As a consequence,
- tabulation can be made in the principal directions only using the first several directions, we call it the tabulation dimension, denoted by n_t.

For convenience of tabulation, we normalize the tabulated components of the composition vector in the principal directions such that the normalized components lie in the range $[0, 1]$ in each direction. For each component j:

$$\tilde{\phi}_j = \left(\hat{\phi}_j - 2\hat{\phi}_{\min,j}\right)/\left(2\hat{\phi}_{r,j}\right), \tag{18}$$

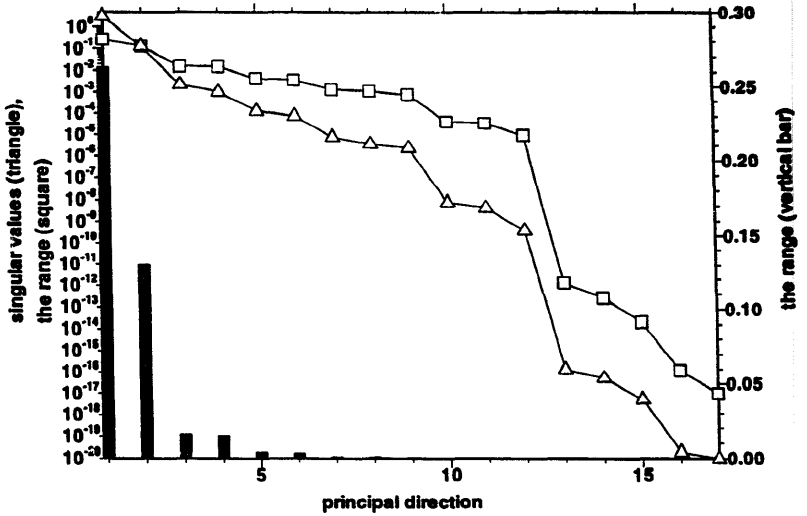

Fig. 2. Distribution of the range and singular values for the methane/air combustion system. Singular values are denoted by triangles. Ranges are denoted by squares in log scale and vertical bars in linear scale.

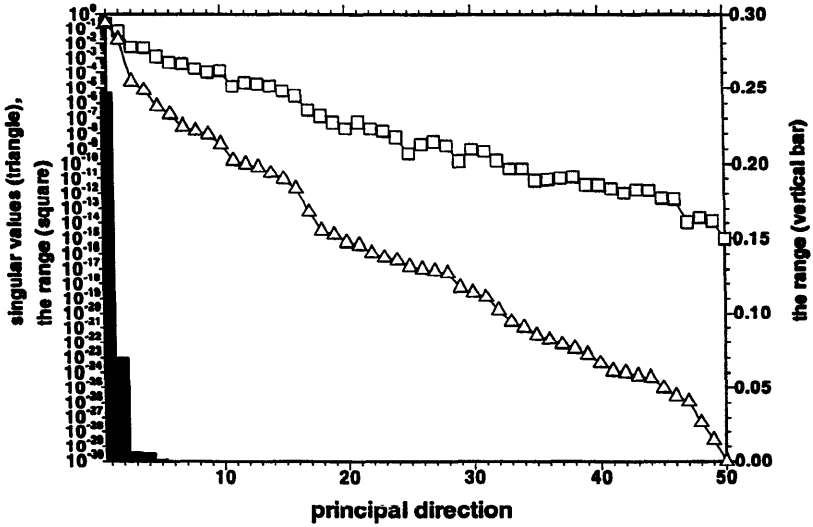

Fig. 3. Distribution of the range and singular values for the natural gas combustion system. Singular values are denoted by triangles. Ranges are denoted by squares in log scale and vertical bars in linear scale.

where $j = 1, 2, \ldots, n_t$, the symbol $\tilde{}$ means normalized. In the equation, 2 is placed to include more points (ideally all accessible points) in the tabulated region. In practical calculations, if $\tilde{\phi}_j$ is less than zero, then it is set to be zero; if $\tilde{\phi}_j$ is greater than one, then it is set to be one.

The following shows the procedure of solving Eqs. 11 and 12 by the operator splitting techniques using the ISATPD method for the chemistry fractional step:

1) given the compositions of two pairing particles at time t, $\phi^{(i)}(t)$ and $\phi^{(j)}(t)$,
2) perform pure mixing according to Eqs. 13 and 14 over the subtime step δt to obtain $\phi^{(i)}_{\text{mix}}$ and $\phi^{(j)}_{\text{mix}}$. The analytic solution is

$$\phi^{(i)}_{\text{mix}} = \phi^{(i)}(t) - \tfrac{1}{2}[\phi^{(i)}(t) - \phi^{(j)}(t)] \times (1 - e^{-2\delta t/\tau_{\text{mix}}}), \quad (19)$$

$$\phi^{(j)}_{\text{mix}} = \phi^{(j)}(t) + \tfrac{1}{2}[\phi^{(i)}(t) - \phi^{(j)}(t)] \times (1 - e^{-2\delta t/\tau_{\text{mix}}}), \quad (20)$$

3) map $\phi^{(i)}_{\text{mix}}$ and $\phi^{(j)}_{\text{mix}}$ to the principal directions according to Eq. 8:

$$\hat{\phi}^{(i)}_{\text{mix}} = \mathbf{U}^T(\phi^{(i)}_{\text{mix}} - \phi^0), \quad (21)$$

$$\hat{\phi}^{(j)}_{\text{mix}} = \mathbf{U}^T(\phi^{(j)}_{\text{mix}} - \phi^0), \quad (22)$$

4) normalize $\hat{\phi}^{(i)}_{\text{mix}}$ and $\hat{\phi}^{(j)}_{\text{mix}}$ by Eq. 18 to get $\tilde{\phi}^{(i)}_{\text{mix}}$ and $\tilde{\phi}^{(j)}_{\text{mix}}$,
5) for each of $\tilde{\phi}^{(i)}_{\text{mix}}$ and $\tilde{\phi}^{(j)}_{\text{mix}}$ search in the table by the ISAT method to see if it is contained in a fine cell. If it is, then return the stored increment of the fine cell back to combustion calculation. Otherwise, the direct numerical integration of Eq. 1 is performed to get the increment. This is then stored as the increment of a new fine cell, and is returned to combustion calculation.

5. RESULTS AND DISCUSSIONS

The performance of the ISATPD method is characterized by its efficiency and accuracy. The efficiency of ISATPD is determined by two parameters. The first one is the upper limit speed-up denoted by r_t, defined by

$$r_t = t_d/t_i, \quad (23)$$

where t_d is the cpu time for doing one direct numerical integration of the governing equation due to chemical reactions, t_i is the cpu time for cell searching and information retrieve using the ISATPD method without doing direct numerical integration. The second one, denoted by r_n, is the ratio of the total number of the direct numerical integrations performed in ISATPD calculations to the total number using direct numerical integration without employing the ISATPD method. The parameter r_n can be written as

$$r_n = n_{\text{rec}}/(Mi_{\text{sub}}), \quad (24)$$

where n_{rec} is the number of the records in the table, M is the number of particles in the PPMSR, and i_{sub} is the number of subtime steps. r_n represents the fraction of the total direct integration in the process of calculation using the ISATPD method. If $r_n = 1$, then all calculations of composition increments are done by direct integration. If $r_n = 0$, then no direct integration is needed: all the increments can be found in the table. So r_n is a parameter which shows how efficient the tabulation is.

There are three kinds of errors involved in this method. The first one is the operator splitting error and the second one is the tabulation error. As in [4], the operator splitting error is defined by

$$\epsilon_{D0} = \langle|\phi_D - \phi_0|\rangle, \quad (25)$$

which is the 2-norms of vectors $\phi_D - \phi_0$,

$$|\phi_D - \phi_0| = \left\{\sum_{i=1}^{n} (\phi_{D,i} - \phi_{0,i})^2\right\}^{1/2}, \quad i = 1, \ldots, n, \quad (26)$$

averaged over the particles in the PPMSR. Here the subscript, D means direct integrations of Eqs. 11 and 12, 0 means direct numerical calculations using zero-order splitting strategy. The average value, $\langle|\phi_D - \phi_0|\rangle$, is defined by

$$\langle|\phi_D - \phi_0|\rangle = \frac{1}{M}\sum_{i=1}^{M} |\phi_D^{(i)} - \phi_0^{(i)}|, \quad (27)$$

where M is the number of particles in the reactor. This is a measure of the error between

the solution from the direct integration of the original full coupled equations and the solution from the direct integration of the zero-order splitting system.

The tabulation error, denoted by ϵ_{0T}, is

$$\epsilon_{0T} = \langle |\phi_0 - \phi_T| \rangle = \frac{1}{M} \sum_{i=1}^{M} |\phi_0^{(i)} - \phi_T^{(i)}|, \quad (28)$$

where the subscript T means the results are calculated using the ISATPD method. Tabulation error indicates how accurate the tabulation method is.

The last error is denoted by ϵ_{DT}, and is defined by

$$\epsilon_{DT} = \langle |\phi_D - \phi_T| \rangle = \frac{1}{M} \sum_{i=1}^{M} |\phi_D^{(i)} - \phi_T^{(i)}|. \quad (29)$$

This is the error that indicates overall how accurate the tabulation method is.

In our calculations the enthalpy is conserved, which means that the nth component of the vector ϕ is a constant. So the errors ϵ_{D0}, ϵ_{0T}, and ϵ_{DT} are the errors of mass fractions. Because the 1-norm of ϕ without the nth component is always unity (the summation of mass fractions is one), so the errors are equivalently normalized quantities.

For all the results reported in this paper, the computer used is an SGI INDIGO workstation.

5.1. The Methane/Air Combustion System

In this section, the results are for the methane/air combustion system with the skeletal mechanism.

5.1.1. General Aspects

For the tests reported in this section, the conditions are: the equivalence ratio is $\varphi = 1.0$; the number of subtime steps in each time step is $n_{\text{sub}} = 5$, which corresponding to the subtime step $\delta t = 1.2 \times 10^{-4}$ s; the mixing time scale is $\tau_{\text{mix}} = 1.0 \times 10^{-3}$ s; the pressure is $p = 1$ atmosphere. The levels are specified according to Method III in Table 1.

Figure 4 shows the average cpu time of one direct numerical integration, $\langle t_d \rangle$, and average cpu time of cell searching and information retrieval using the ISATPD method, $\langle t_i \rangle$, and

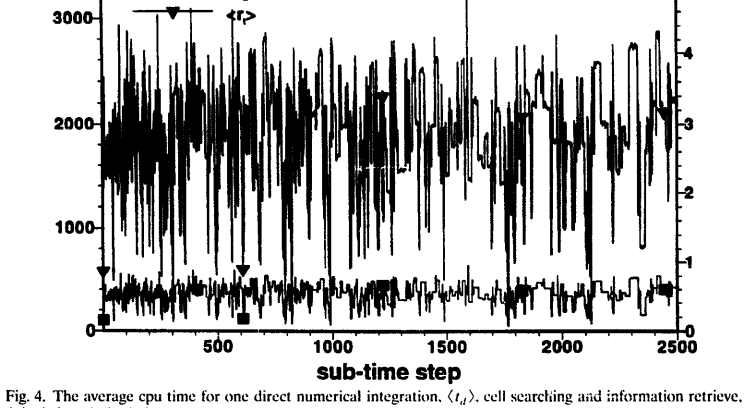

Fig. 4. The average cpu time for one direct numerical integration, $\langle t_d \rangle$, cell searching and information retrieve, $\langle t_i \rangle$, $\langle r_t \rangle = \langle t_d \rangle / \langle t_i \rangle$, as functions of the sub-time step.

the ratio, $\langle r_t \rangle = \langle t_d \rangle / \langle t_i \rangle$, as functions of subtime steps. For continuity of the curve, on the subtime step at which no direct numerical integation is carried out, $\langle t_d \rangle$ is just given the previous value. From this plot one can see that except in the beginning few steps, where $\langle t_i \rangle$ increases, $\langle t_i \rangle$ is statistically constant. The value of it is about 2.8×10^{-4} s. While at the same time the number of records in the table, n_{rec} increases from 0 to about 2500. What this tells us is that the cell searching and information retrieval time is independent of the number of records in the table. This is a very important property of the ISATPD method. The value of $\langle t_d \rangle$ is about 0.6 s. On average, $\langle r_t \rangle$ is about 2000 which means that to get the increment of the composition of a particle, on the average, by ISATPD method is about 2000 times faster than by direct numerical integrations.

Plotted in Fig. 5 are the number of direct numerical integrations performed at each subtime step, or the number of records added on each subtime step, n_a; the parameter r_n defined by Eq. 24; the total number of records in the table, n_{rec}. One important observation here is that as time goes on, the number added on each subtime step n_a, decreases rapidly. After some time steps, most of the time, n_a is either zero or one which means that all the particles, or 99 of the total 100 particles, in the PPMSR have compositions that lie within fine cells in the table. One very important property of the table is that the total number of records in the table is small. As the figure shows, at subtime step 2500, n_{rec} is about 2600. The parameter r_n decreases rapidly, and asymptotically approaches zero.

To test the efficiency, the calculation is advanced to subtime step 2×10^6. This corresponds to the number of queuing particles of 2×10^8, which is comparable to the total number of queuing particles in PDF calculations of turbulent combustion. Plotted in Fig. 6 are n_{rec}, r_n, t_c, and r_s. Here t_c is the cpu time to perform chemistry by the ISATPD method, which includes the cpu time to do cell searching and information retrieving and the cpu time to do direct numerical integration in the case that no fine cells are found for query

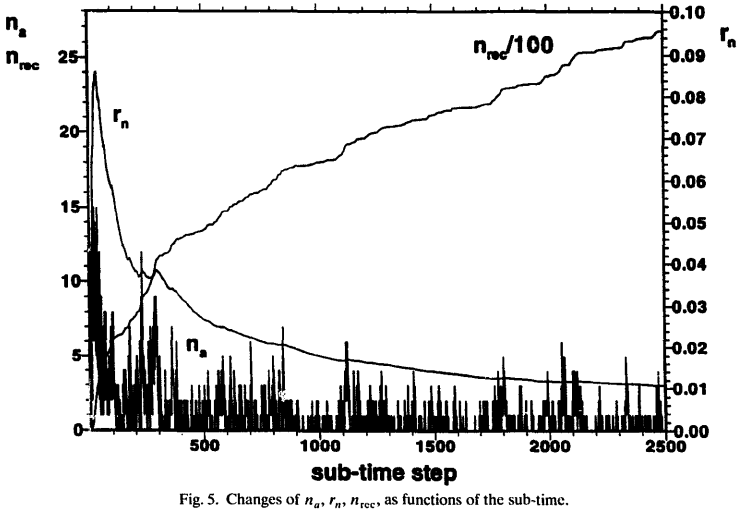

Fig. 5. Changes of n_a, r_n, n_{rec}, as functions of the sub-time.

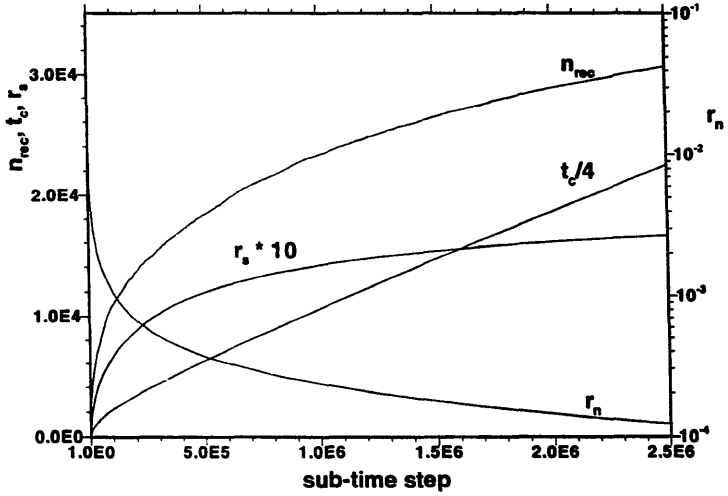

Fig. 6. Changes of r_n, n_{rec}, t_c and r_s as functions of the sub-time step.

particles. r_s is the practical speed-up obtained, which is defined by the following:

$$r_s = (i_{sub} \times 100 \times 0.6)/t_c, \tag{30}$$

where i_{sub} is the number of subtime steps, there are 100 particles in the reactor, and the average cpu time to perform one direct numerical integration of the governing equation due to chemical reactions is about 0.6 second. From this figure, we can see that the total number of records in the table is still small, at sub-time step 2×10^6, $n_{rec} = 30{,}699$. Consistent with Fig. 5, r_n decreases, the value of it at subtime step 2×10^6 is 2.81×10^{-4}. At the same subtime step, the speed-up, r_s, is 1665, and the cpu time, t_c, is 9.00×10^4 seconds (25 h). If the calculation is performed by direct numerical integration without using the ISAPD method, then the cpu time is $r_s \times 25 = 1665 \times 25 =$ 41,625 h, or 4.75 years. In other word, the ISATPD method decreases the cpu time from about 5 years to about one day! What this tells us is that the ISATPD method is a very efficient method.

There are two major reasons for the number of records in the table being small. The first one is that the ISATPD method is efficient. Doing tabulation in the principal directions of the composition space ensures that the table is of low dimensionality even though the dimensionality of the composition space may be high. The second reason is due to the nature of the combustion system—the accessed region is limited in narrow regions, which can be seen from Fig. 7. In this figure, the total fractional change of temperature, η_t, is defined by

$$\eta_t = \frac{T(t + \delta t) - T(t)}{T(t)}, \tag{31}$$

where $T(t + \delta t)$ is the temperature of a particle at time $t + \delta t$, $T(t)$ is the temperature at time t. η_t includes the change due to mixing and the change due to chemical reactions. Figure 7 is a scatter plot of η_t versus $T(t)$ for the records in the table. One can clearly see from this picture that the points are not uniformly distributed in the region, instead they are scattered along curves. There are two basic processes in combustion which change the composition of a particle—the molecular mixing and the chemical reaction. In the PPMSR, mixing can occur between any possible combination of

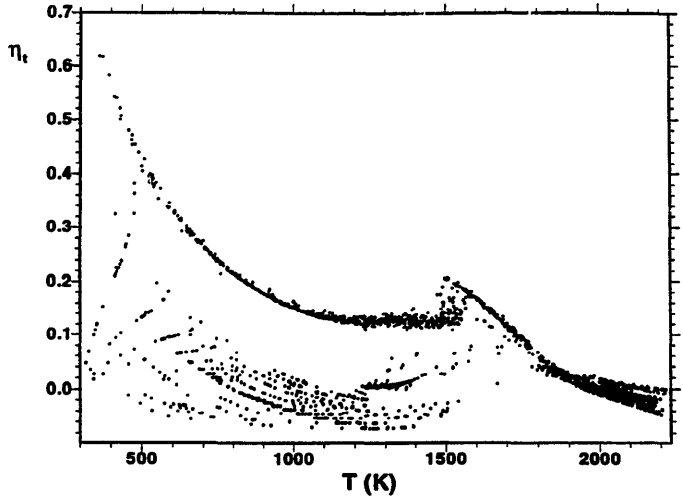

Fig. 7. Scatter plot of η_t versus temperature T.

pairing particles. So as a whole, the mixing tends to scatter composition points in the composition space. While for the chemical reaction, as discussed in [8], it draws the trajectory of the composition point in the composition space toward low-dimensional manifolds. If the chemical reaction is strong, then the composition points are attracted to low dimensional manifolds, thus they are restricted to narrow regions.

In Fig. 8, the fractional change of temperature due to chemical reactions, denoted by η_r, is defined by

$$\eta_r = \frac{T(t + \delta t) - T_{\text{mix}}}{T_{\text{mix}}}, \tag{32}$$

where T_{mix} is the temperature of a particle after the mixing fractional step. Figure 8 is a scatter plot of η_r versus T_{mix} for the records in the table. η_r indicates how much energy is released in each subtime step. As suggested in [11], in the calculations of combustion using operator splitting methods, energy release should be controlled by no more than 10–20%. Figure 8 shows that η_r satisfies this requirement. This means that the value of the sub-time step δt used in the calculation is a proper one.

Figure 9 shows the distribution of records in the table. Plotted in this figure is the fraction of the records with the temperature T in the range of $[T, T + 100)$ as a function of T. In the figure, I-1000 means the distribution of the first 1000 records, I-2000 the first 2000 records, and so on. We can see that as the number of records increases, the distribution approaches as fixed pattern. The fraction in the low regions ($T < 600$ K), and highest temperature ($T > 2200$ K) are low. The local minimum value of the distribution is at about 1700 K, which corresponds to the maximum change region shown in Fig. 8. The peak of the fraction occurs at the temperature about 2000 K.

The errors are shown in Fig. 10. The operator splitting error ϵ_{D0} is about 5.5×10^{-4}, the tabulation error ϵ_{0T} is about 5×10^{-4}. The overall error ϵ_{DT} is about 8×10^{-4}. There is a peak for the operator splitting error ϵ_{D0} and the overall error ϵ_{DT} at time step 12, which is about 2.5×10^{-3}. But for the tabulation error

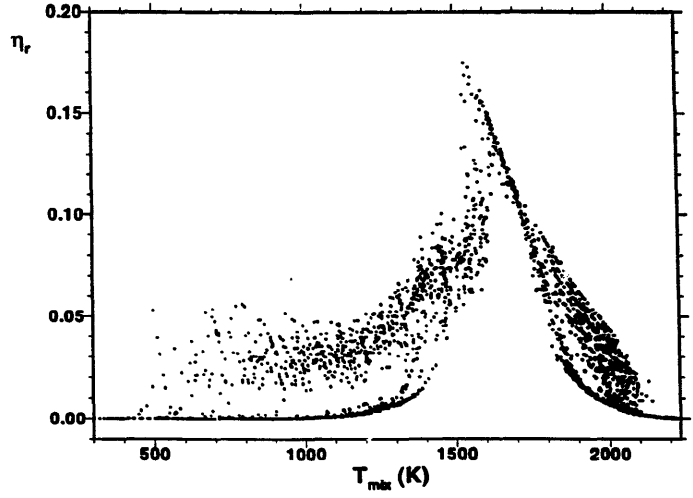

Fig. 8. Scatter plot of η_r versus temperature T_{mix}.

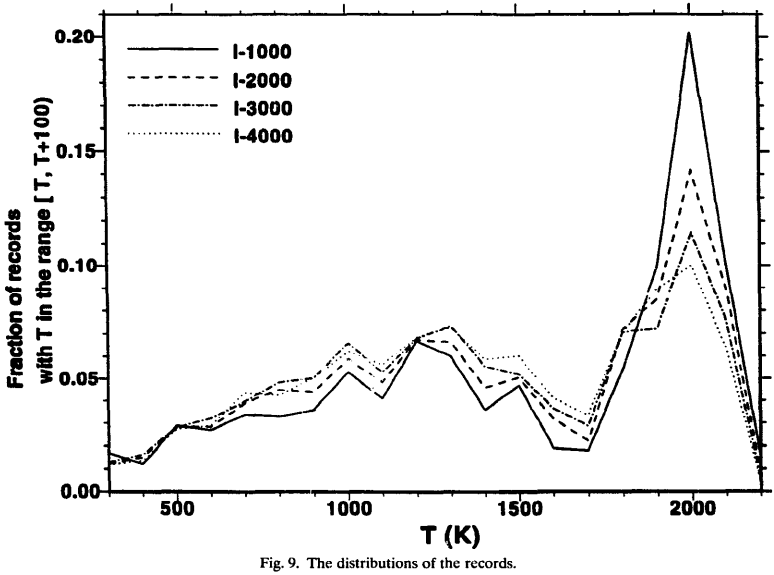

Fig. 9. The distributions of the records.

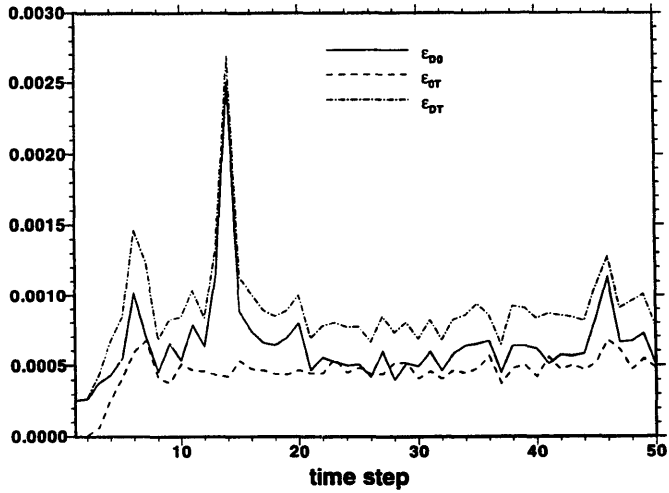

Fig. 10. The splitting errors, ϵ_{D0}, the tabulation error, ϵ_{0T}, and the overall error ϵ_{DT}, as functions of time step.

ϵ_{0T}, there is no such peak. This figure tells us that the tabulation error is small. The overall error of the ISATPD method is close to the operator splitting error and is controlled by the operator splitting error.

Figure 10 shows how accurate the composition vector as a whole is. We can plot the average mass fractions of particles in the PPMSR calculated by direct integration with the operator splitting strategy and the ISATPD method, and see how accurate the tabulation method is for each individual species. In all the accuracy discussions in this paper, the comparison is made between the direct numerical integration using the operator splitting strategy (solid lines) and the results from the ISATPD method (dashed lines). The mean mass fraction plots are shown in Figs. 11 and 12. For stable species like H_2O, CO_2, CH_4, CO, and O_2, the agreement is excellent. For major radicals, O, OH, and H, the agreement is also excellent. Even for minor species (such as HCO) with mass fractions as low as 10^{-7}, the agreement is very good. As discussed before, the corresponding efficiency is very high. So excellent agreement can be obtained with very high efficiency by the ISATPD method.

5.1.2. The Influence of Levels

Three different level specification methods (shown in Table 1) are tested. The efficiencies of these methods are shown in Fig. 13. Since the computer cpu time of cell searching and information retrieve for the methods is about the same, it is not included in this figure and is neglected in the following discussions. It can be seen that Method I has the highest efficiency, then Method III, and then Method II. The differences of the efficiencies of these methods are small, especially at a large number of subtime steps. All of these methods are very efficient. The accuracy for representative species is shown in Fig. 14. They all provide excellent calculations for the stable species and radicals. For minor species, the agreement is still very good.

One important thing to be noted is that the tabulation dimension, n_t, for Methods I and II, is only 3. With the excellent accuracies obtained and the increasing in the accuracy just

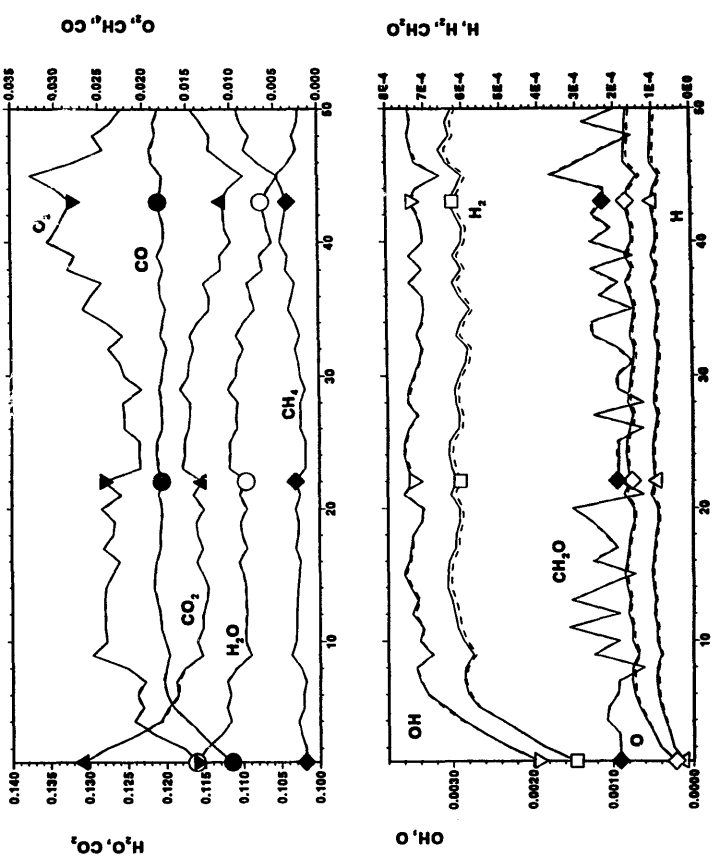

Fig. 11. Mean mass fractions of H_2O, CO_2, O_2, CH_4, CO, OH, O, H, H_2 and CH_2O as functions of time step. Solid lines, direct integration; dashed lines, the ISATPD method.

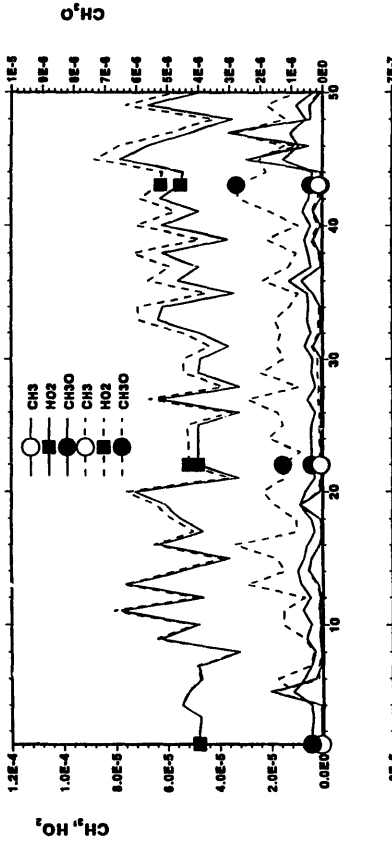

Fig. 12. Mean mass fractions of CH_3, HO_2, CH_3O, H_2O_2, and HCO as functions of time step. Solid lines, direct integration; dashed lines, the ISATPD method.

TABLE I

Methods of Level Specification

Direction, i		1	2	3	4	5	6
Level, l_i	Method I	7	6	4			
	Method II	8	7	5			
	Method II	7	6	4	4	4	2

by increasing the level, we can conclude that in the principal directions of the composition space, the movement of the trajectory of the composition point is essentially restricted to the first three dimensions. What this means mathematically is that the number of linearly independent relationships is essentially three for the premixed methane/air combustion system with the skeletal mechanism. There are five linearly dependent relationships for this system (four element conservations, and one enthalpy conservation). The remaining nine ($= 17 - 3 - 5$) relationships, even though not absolutely linearly dependent, are almost linearly dependent as it is indicated by the singular value decomposition of the matrix C (see Fig. 2).

The idea of the ISATPD method is similar to that of the reduced mechanism method and the ILDM method in the sense that they all assume or find a low-dimensional space. For the reduced mechanism method, this low-dimensional space is found by assuming steady-state for some species and partial equilibrium for some reactions [6, 7]. For the ILDM method, the low-dimensional manifold is found by studying time scales at each composition space point [8]. For the ISATPD method, the low-dimensional space is found by studying the singularities of the matrix C. The existence of such a low-dimensional space is due to the fact that the number of the linearly independent relationships of composition components is low. The basic thinking of the ISATPD method is essentially different from chemistry simplification methods. For the methods of chemistry simplification, such as the reduced mechanism method and ILDM methods, integrations and the tabulation are all done in the same low-dimensional space. All possible regions are tabulated. For the ISATPD method, the tabulation is done only in the low-dimensional

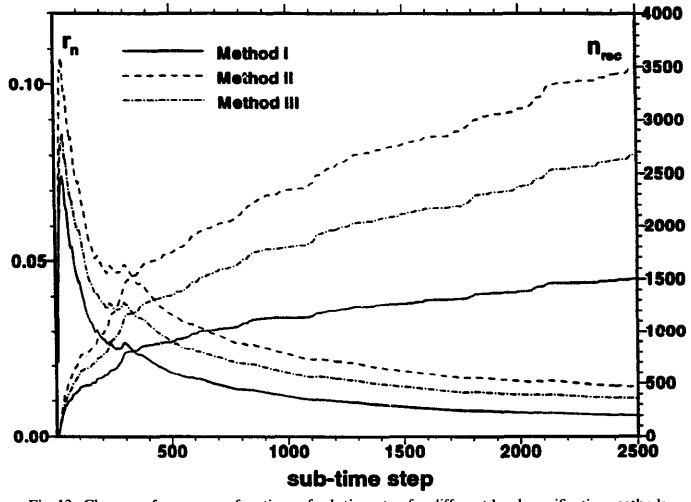

Fig. 13. Changes of r_n, n_{rec}, as functions of sub-time step for different level specification methods.

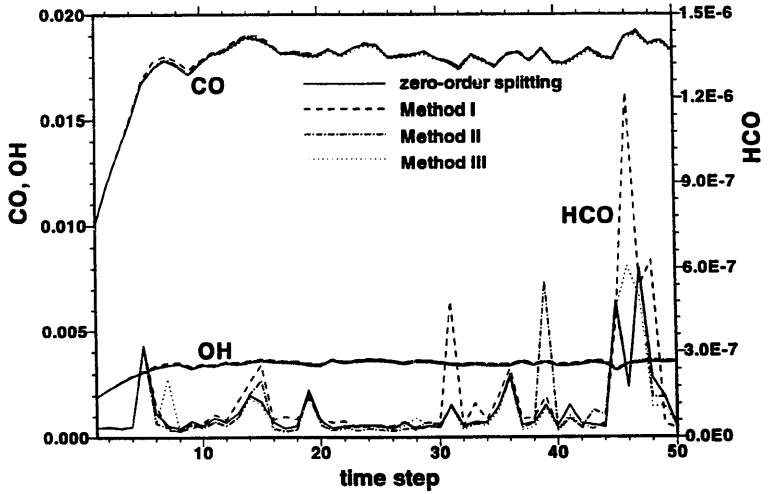

Fig. 14. Means mass fractions of CO, OH, and HCO for different level specification methods. Solid lines, direct integration (zero-order splitting).

space, while the integration is done using the given mechanism. No simplifications are made to the chemistry. And more, the tabulation is done *in situ*. Only the accessed composition regions are tabulated. So the ISATPD method is an accurate and yet efficient method.

The other very important property of the ISATPD method that should be noted here is that the number of records of the table is not a strong exponential function of either the level, or the dimension of the table, as it is in the case for conventional tabulation methods. As Fig. 13 shows, increasing the level in each direction by one, the number of records only increases by a factor of 2.3, instead of $2^3 = 8$. While increasing the dimension of the table from 3 to 6, the increase in the number of records is by a factor of 1.8, which is much smaller than $2^{4+4+2} = 2^{10} = 1024$. This means that if one is not satisfied with the accuracy of a calculation, one can easily increase the accuracy of the calculation by either specifying high levels, or by increasing the tabulation dimension, without much increase in the number of records. This is another extremely important property of the ISATPD method. For conventional tabulation method, increasing in the dimension of the table, or the resolution in each direction, will increase the number of cells dramatically.

5.1.3. Tests for Different Equivalence Ratios

Influences of the equivalence ratio φ are studied in this section. Calculations are performed for lean and rich combustion with equivalence ratios, $\varphi = 0.6$, and 1.5, respectively. The level specification method is Method III shown in Table 1. Accuracies for both calculations are as good as the calculation at the stoichiometric condition. To save space, we do not present the figures here. Their efficiencies are shown in Fig. 15. It can be seen that for both cases, the same characteristics for $\varphi = 1.0$ are remained unchanged. The parameter r_n approaches zero as the number of time steps increases. Compared with the case $\varphi = 1.0$, the number of records n_{rec} is large. The reason can be seen from the scatter plots of η_i (Eqs. 31) in Fig. 16 for $\varphi = 0.6$, and Fig. 17 for $\varphi = 1.5$. Compared with the corresponding plot for $\varphi = 1.0$ (Fig. 7), the points are more widely scattered, especially for the case $\varphi = 0.6$ where

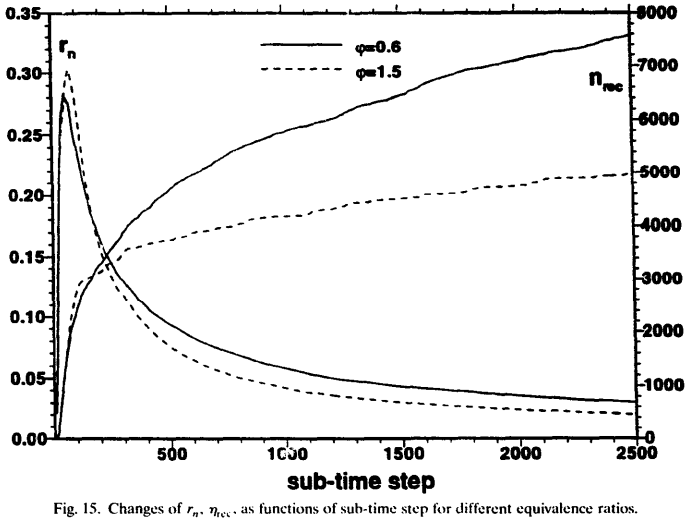

Fig. 15. Changes of r_n, η_{rec}, as functions of sub-time step for different equivalence ratios.

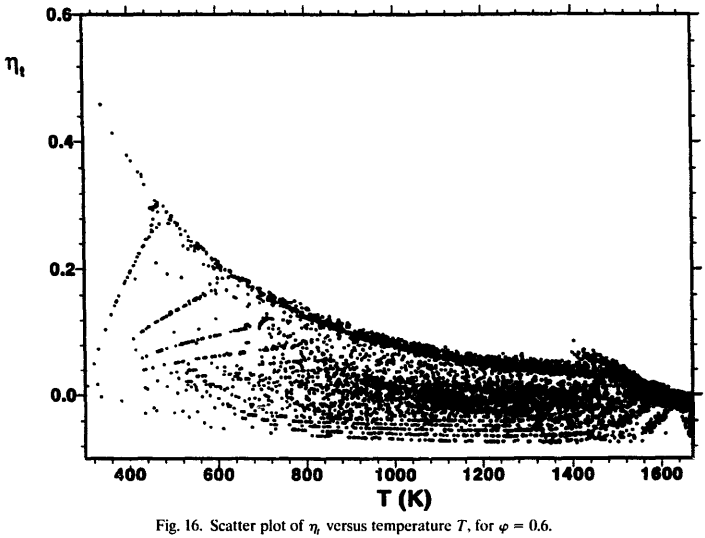

Fig. 16. Scatter plot of η_t versus temperature T, for $\varphi = 0.6$.

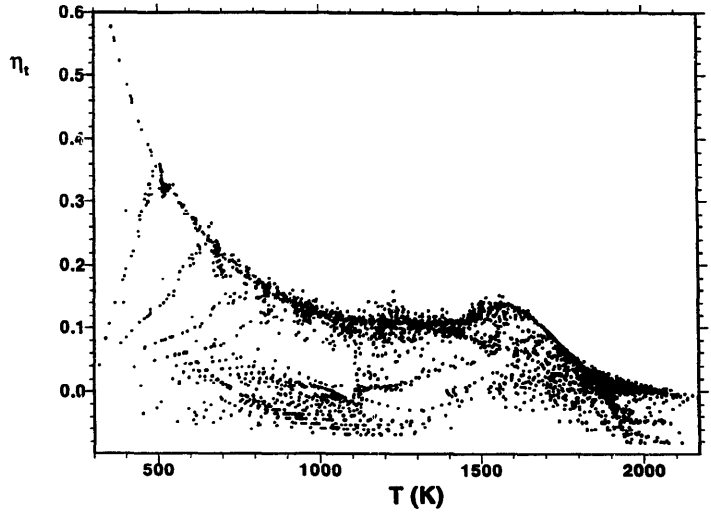

Fig. 17. Scatter plot of η_t versus temperature T, for $\varphi = 1.5$.

the process occurs in the low temperature region. As a result, more fine cells are needed to cover the accessed region. So the number of records n_{rec} increases.

5.1.4. Test for Different Mixing Time Scales

Tests of the influences of the mixing time scale are performed for the stoichiometric condition with level specification Method III. Efficiency parameters are plotted in Fig. 18. Scatter plots of temperature changes η_t are shown in Fig. 19 for $\tau_{mix} = 5 \times 10^{-3}$ second, and in Fig. 20 for $\tau_{mix} = 10^{-4}$ s. Figures showing the accuracies are not presented here for the sake of space saving. Accuracies are still excellent. Figure 18 shows that the method is still very efficient. Compared to the case with the mixing time scale $\tau_{mix} = 10^{-3}$ s, the case with $\tau_{mix} = 5 \times 10^{-3}$ s has more records in the table, while for the case with $\tau_{mix} = 10^{-4}$ s, the number of records is about 600 more. There are two ways the mixing influences the combustion of a PPMSR. As the mixing time scale decreases, or the mixing increases, mixing scatters the composition point wider in the composition space, but at the same time, mixing enhances combustion, which has the effect of attracting the composition points toward low dimensional manifolds. As the mixing time scale increases, the reverse influences occur. What these figures tell us is that at the conditions tested, the enhancement of combustion due to increasing mixing is more important than the scatter effects of increasing mixing.

5.1.5. Tests at High Pressure

One test calculation is performed at the pressure $p = 50$ atmosphere, $\varphi = 1.0$, $\delta t = 1.2 \times 10^{-4}$ s, $\tau_{mix} = 10^{-3}$ s. As pressure increases, reaction rates also increase. Since the mixing time scale remained unchanged, so the effects of mixing are also not changed. The accessed regions become more simple and narrow, as they are shown in Fig. 21. The efficiency parameters are plotted in Fig. 22. It is ten times more efficient than at one atmosphere. Mass fractions for some typical species are shown in Fig. 23. We can see that even though the agreement is not as good as the calculations at one atmosphere. But it is still very good. And

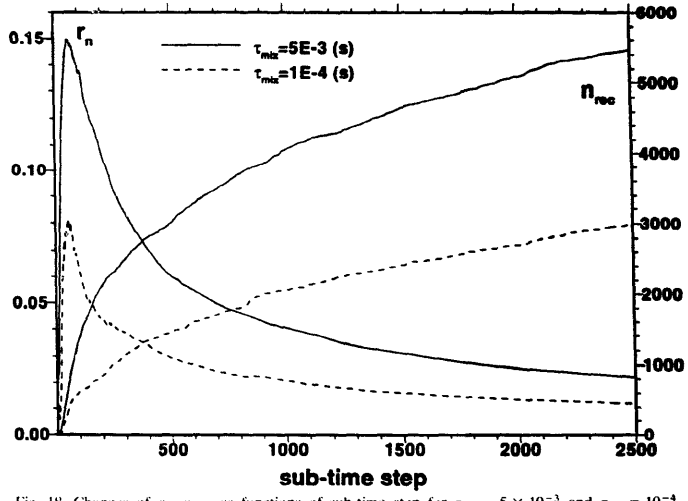

Fig. 18. Changes of r_n, η_{rec}, as functions of sub-time step for $\tau_{mix} = 5 \times 10^{-3}$ and $\tau_{mix} = 10^{-4}$ second.

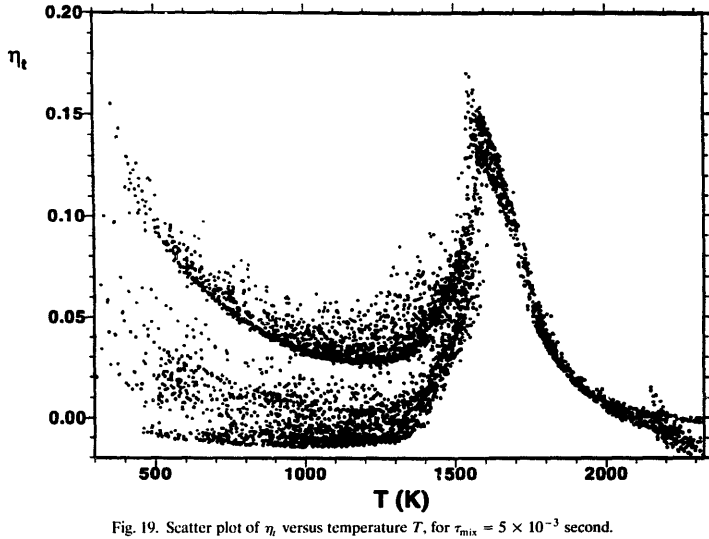

Fig. 19. Scatter plot of η_t versus temperature T, for $\tau_{mix} = 5 \times 10^{-3}$ second.

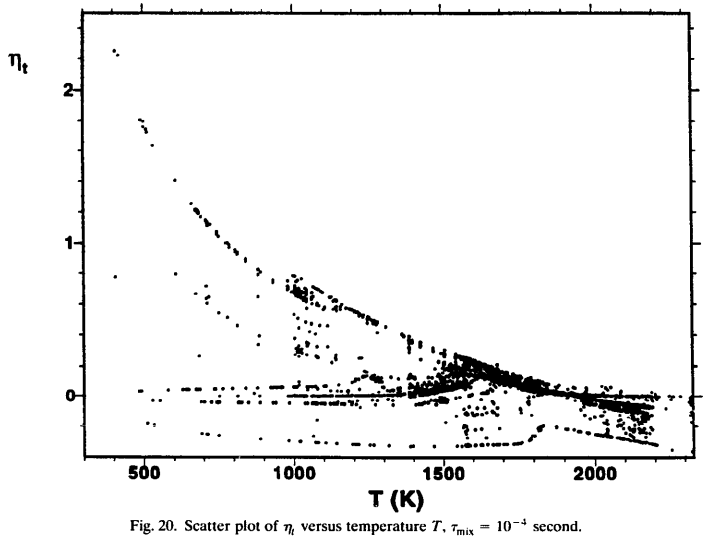

Fig. 20. Scatter plot of η_t versus temperature T, $\tau_{mix} = 10^{-4}$ second.

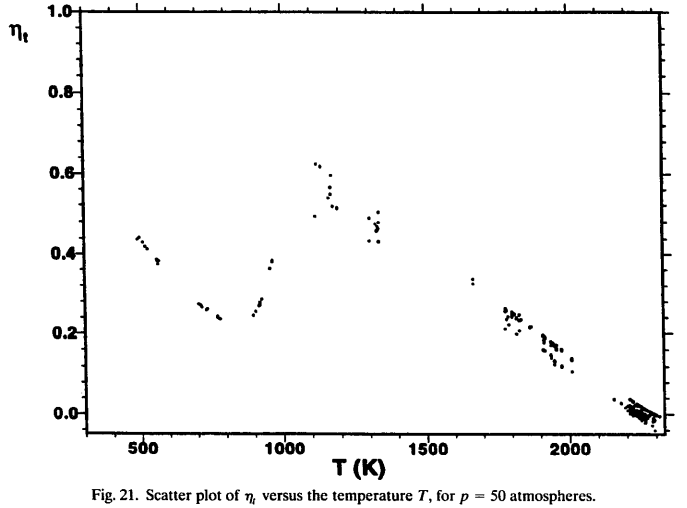

Fig. 21. Scatter plot of η_t versus the temperature T, for $p = 50$ atmospheres.

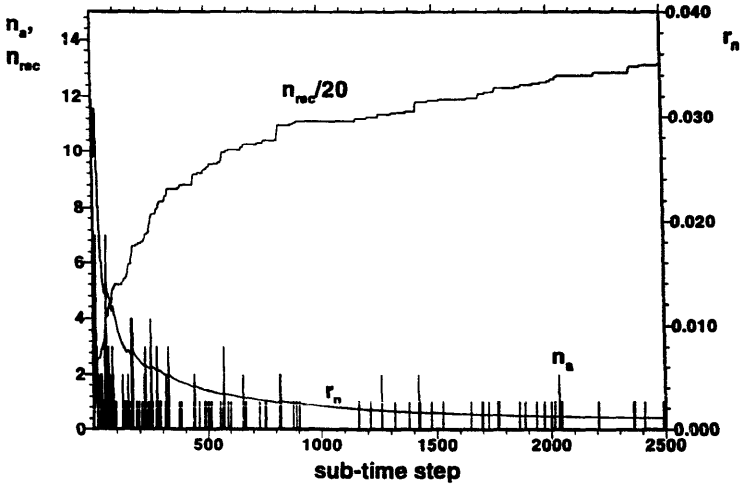

Fig. 22. Changes of n_a, r_n, n_{rec}, as functions of sub-time step, for $p = 50$ atmospheres.

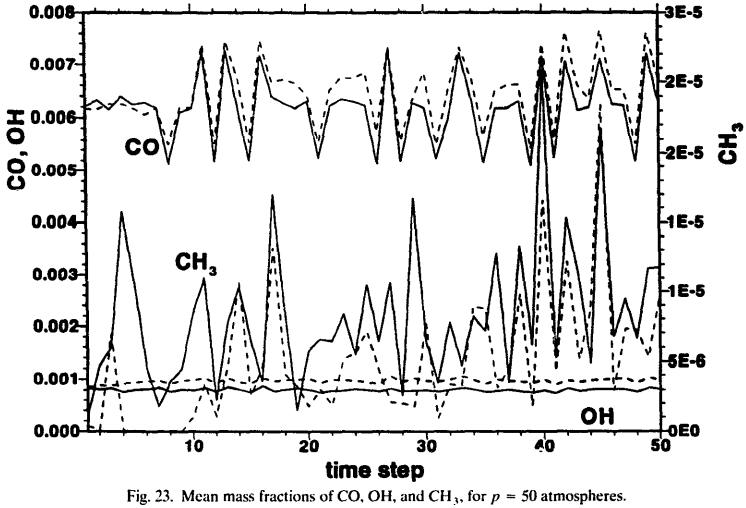

Fig. 23. Mean mass fractions of CO, OH, and CH_3, for $p = 50$ atmospheres.

more, since we have a very small number of records here, so we can increase the accuracy easily by specifying high levels in the tabulation.

5.2. The Natural Gas Combustion with the GRI 2.11 Mechanism

The ISATPD method has been shown in the above section to be a very efficient and accurate method for the premixed methane/air combustion system with the skeletal mechanism having 16 species. Now, how does it perform for the natural good combustion system with the GRI 2.11 mechanism which has 49 species?

One calculation is done with the following parameters, $p = 1$ atmosphere, $\varphi = 1.0$, $\delta t = 1.2 \times 10^{-4}$ s, $\tau_{\text{mix}} = 10^{-3}$ s. The composition of the natural gas is taken to be 81% CH_4, 4% C_2H_6, and 15% N_2, by volume. As shown in Fig. 3, the distribution of the range of the principal directions is similar to those for the methane/air combustion system with the skeletal mechanism. We use the level specification Method III as shown in Table 1. Efficiency parameters are shown in Fig. 24. From this figure one can see the same properties as for the methane/air combustion system with the skeletal mechanism: the number added to the table is either zero or one for most of the time after some subtime steps, the ratio r_n asymptotically approaches zero as the number of sub-time steps increases, the total number of records in the table n_{rec} is a small number, at sub-time step 2500, n_{rec} is about 2000, which is even less than that for the methane/air combustion system with the skeletal mechanism.

With respect to the computer time, we can say that the cell searching and information retrieve time, denoted by t_i, is about the same as that for the methane/air combustion system reported in the previous section since the same tabulation dimension, and the same level specification are used. The value of t_i is about 2×10^{-4} s. The average time to perform one direct numerical integration here is about 30 s, so $r_i = 30/2 \times 10^{-4} = 1.5 \times 10^5$. That means, on average, to get the increment of the compo-

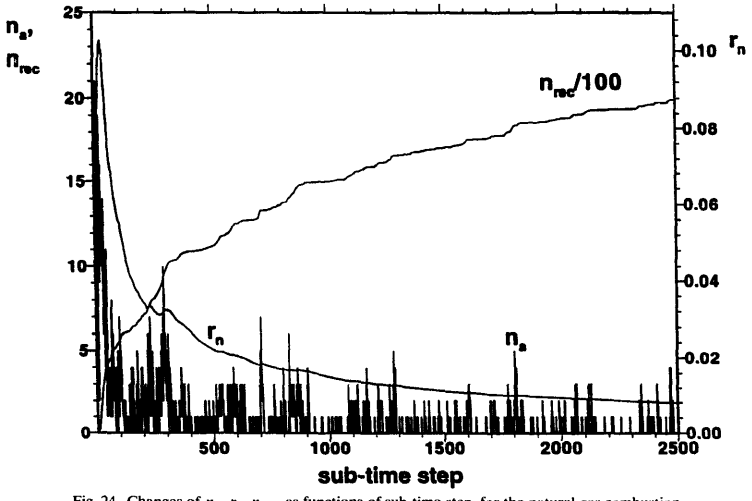

Fig. 24. Changes of n_a, r_n, n_{rec}, as functions of sub-time step, for the natural gas combustion.

sition of a particle by the ISATPD method is about 1.5×10^5 times faster than by direct numerical integrations for the natural gas combustion system with the GRI 2.11 mechanism.

The tabulation error ϵ_{0T} (Eq. 28) is shown in Fig. 25. Also shown in this figure is the corresponding tabulation error for the methane/air combustion system with the skeletal mechanism. We can see that the tabulation error for the natural gas combustion system with the GRI 2.11 mechanism is still very small, which is about 4×10^{-4}. The tabulation errors for the two combustion system are about the same. This means that the accuracy of the ISATPD method is independent of the original dimension of the composition space.

The accuracy of this method for each individual species is indicated in Figs. 26 and 27. Excellent results are obtained for the stable species, CO_2, H_2O, O_2, CO, CH_4, C_2H_6, and importantly, NO, NO_2, the radicals O, OH, H, CH_3, etc. Note that for species with mass fractions as low as 10^{-9} (such as N, NH), or even 10^{-11} (as H_2CN), the agreement is still very good.

Calculations for the natural gas combustion system with the GRI 2.11 mechanism under different conditions are not performed. But we can safely state that the properties observed in the previous section for the methane/air combustion system can still be observed for the natural gas combustion system since the fundamental processes are the same.

6. CONCLUSIONS AND FUTURE WORK

The following conclusions based on the discussions above can be drawn:

1) The *in situ* adaptive tabulation (ISAT) method is very efficient—the cell searching and information retrieval takes only about 10^{-4} s on an SGI INDIGO workstation, and it is independent of the number of records in the table.
2) In the principal directions of the composition space the trajectory of the composition point is essentiallv restricted to a low dimensional space, despite the fact that the original composition dimension may be very high.

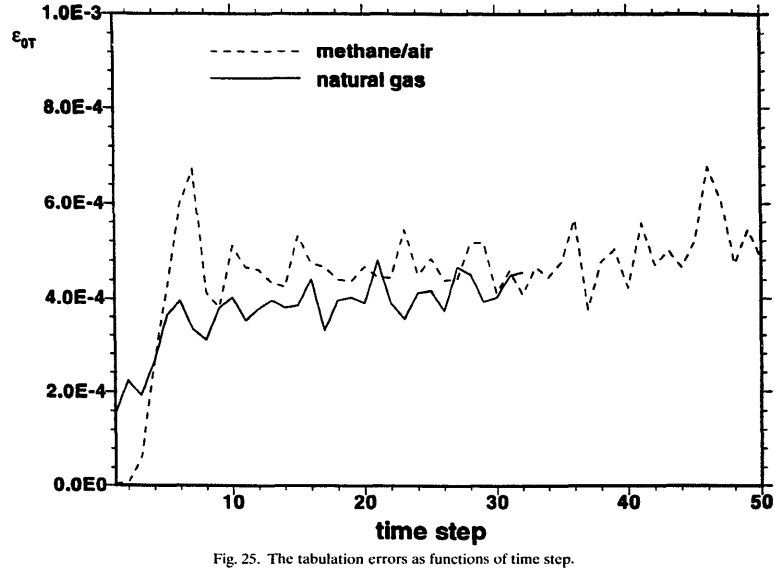

Fig. 25. The tabulation errors as functions of time step.

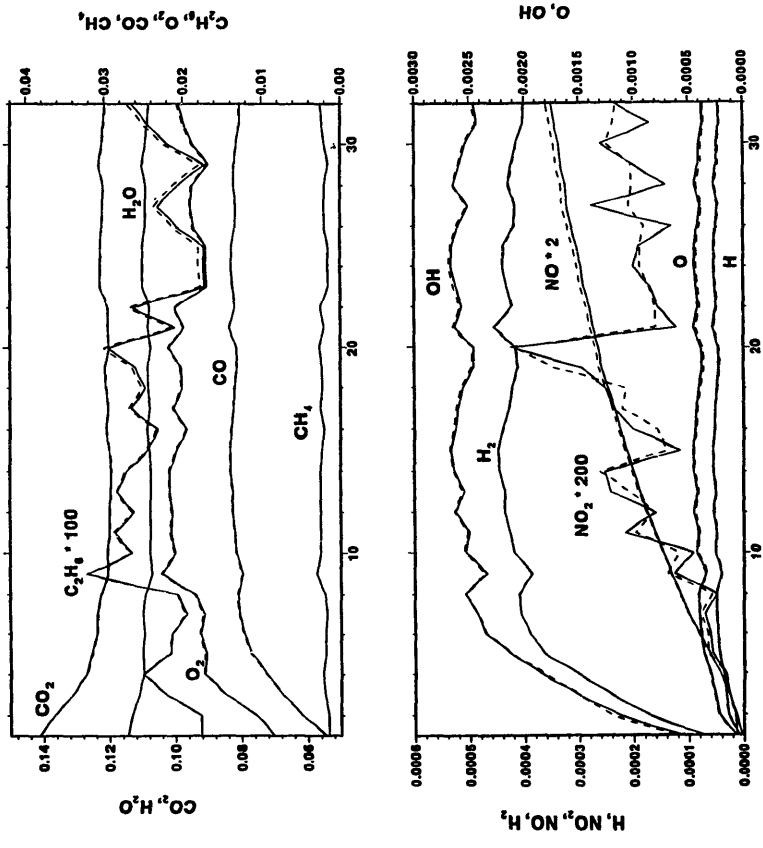

Fig. 26. Mean mass fractions of CO_2, H_2O, C_2H_6, O_2, CO, CH_4, H, NO_2, NO, H_2, O and OH as functions of time step for the natural gas combustion.

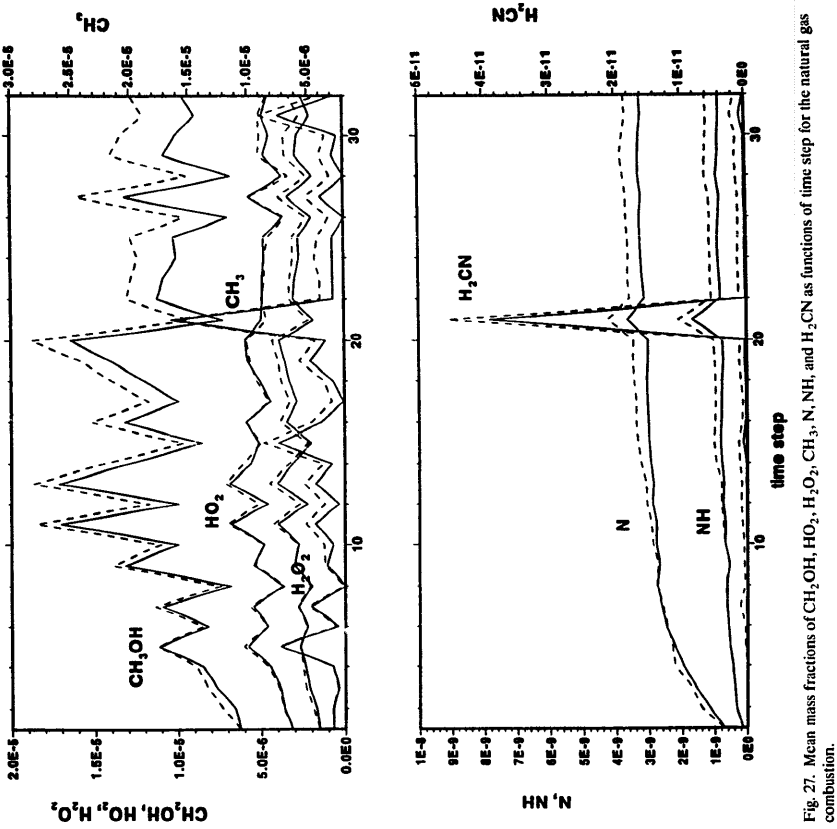

Fig. 27. Mean mass fractions of CH_2OH, HO_2, H_2O_2, CH_3, N, NH, and H_2CN as functions of time step for the natural gas combustion.

3) The *in situ* adaptive tabulation in principal directions (ISATPD) method is very efficient—the number of records added on each subtime step is either zero or one most of the time, the total number of records in the table is small. The reason for this is that the ISATPD method only tabulates the accessed regions, the tabulation is done in a low-dimensional table, and the accessed region is narrow.
4) The ISATPD method is also very accurate —not only can it provide excellent calculations for stable major species, but also for species with very low mass fractions (as low as 10^{-11}). This is due to the fact that the increment is calculated by the direct numerical integration of the governing equations with detailed mechanism, no simplification is made to the mechanism.
5) The total number of records in the table is not an exponential function of either the level or the dimension of the table. The importance of this property is that higher accuracy can be achieved without much increasing in the number of records, or decreasing in the efficiency of this method.
6) Weak chemical reactions decrease the efficiency of the method.
7) Strong mixing tends to scatter the composition points in the wider region, but at the same time it enhances the combustion. Overall, increasing in mixing only increases the number of records by a very small number.
8) The efficiency of the ISATPD method in terms of the records, and the accuracy of this method, is independent of the dimension of the original composition space. In terms of saving in computer time, the ISATPD method is even more efficient when the dimension of the composition space is high.

The test calculations show the high efficiency and accuracy of the ISATPD method for premixed pairwise mixing stirred reactors. The ISATPD method is designed to be capable of doing adaptation. The test calculations are performed without adaptation. Even though, high efficiency is obtained. In future work, the way to do adaptation will be developed. The implementation of the ISATPD method in practical combustion calculations, laminar and turbulent, is expected in future work. The implementation and performance of the ISATPD method for the diffusion pairwise mixing stirred reactors (DPMSR) will be furnished in the near future.

This paper was prepared with the support of the U.S. Department of Energy, Morgantown Energy Technology Center, Cooperative Agreement No. DE-FC21-92MC29061.

REFERENCES

1. Dixon-Lewis, G., David, T., Gaskell, P. H., Fukutani, S., Jinno, H., Miller, J. A., Kee, R. J., Smooke, M. D., Peters, N., Effelsberg, E., Warnatz, J., and Behrendt, F., *Twentieth Symposium (International) on Combustion*, The Combustion Institute, Pittsburgh, 1984, p. 1893.
2. Correa, S. M., Gulati, A., and Pope, S. B., *Twenty-fifth Symposium (International) on Combustion*, The Combustion Institute, Pittsburgh, 1994, p. 1167.
3. Smooke, M. D., Mitchell, R. E., and Keyes, D. E., *Combust. Sci. Tech.*, 67:85 (1989).
4. Yang, B. and Pope, S. B., *Combust. Flame*, 112:17–32 (1997).
5. Pope, S. B., *Twenty-Third Symposium (International) on Combustion*, The Combustion Institute, Pittsburgh, 1990, p. 591.
6. Peters, N., in *Numerical Simulation of Combustion Phenomena*, Lecture Notes in Physics, Springer-Verlag, 1985, R. Glowinski, B. Larrouturou, R. Teman, Eds., Vol. 241, p. 90.
7. Smooke, M. D. (Ed.), *Reduced Kinetic Mechanisms and Asymptotic Approximation for Methane-Air Flames*, Lecture Notes in Physics, Springer-Verlag, 1991, Vol. 384.
8. Maas, U. and Pope, S. B., *Combustion and Flame*, 88:239–264 (1992).
9. Yanenko, N. N., *The Method of Fractional Steps*, Springer-Verlag, Berlin, 1971.
10. Golub, G. H. and Van Loan, C. F., *Matrix Computations*, 2nd ed., Johns Hopkins University Press, Baltimore, 1989.
11. Oran, E. S. and Boris, J. P., *Prog. Energy Combust. Sci.* 7:1 (1981).

Received 29 July 1996; accepted 12 February 1997